S. Afr. J. Chem., 2021, **75**, 106–110
https://journals.co.za/content/journal/chem/

Truncated Edge Cuprous Oxide Cube Architecture for Reduction of Nitrophenols

Elizabeth Erasmus

Department of Chemistry, University of the Free State, Bloemfontein 9300, South Africa

Received 07 February 2020, revised 26 November 2020, accepted 24 December 2020

ABSTRACT

Truncated cubic Cu-oxide nanocrystals with edge lengths of *ca.* 600 nm were prepared employing the low-cost copper (II) chloride as the precursor. XRD revealed that the truncated cubic Cu-oxide nanocrystals are present in both the Cu^{I} and Cu^{0} state. XPS characterisation gives insight into the amount of each state present in the as-prepared, oxidised, reduced and recovered catalyst species. The catalytic activity of the truncated cubic Cu-oxide nanocrystals was tested for the reduction of nitrophenols using $NaBH_4$. After one catalytic cycle of the reduction of 4-nitrophenol, the activity almost halved. The SEM images revealed that the recovered catalyst showed some disfigurement of the structure, and XPS confirmed the reduction of the Cu^{I} to metallic Cu^{0}.

KEYWORDS

Cu-oxide, truncated cubic nanocrystal, nitrophenol, catalysis, X-ray photoelectron spectroscopy.

1. Introduction

Metal oxide nanostructures are of great interest due to their enhanced chemical, physical, optical, electromagnetic and electronic properties in contrast to bulk metal oxides.[1–3] These improved properties render them to be very versatile for many uses in different technological applications, including the chemical-, pharmaceutical industries, water treatment, food technology, and energy. In addition, due to the structural stability and diversity, metal oxides are regarded as excellent heterogeneous supports for the active catalyst particles. Due to the variety of oxidation states the metal oxide can adopt, metal oxides can be catalytically active themselves,[4] especially during redox reactions.

It has been shown that there is a correlation between low bandgap energy (energy required to stimulate a valence electron to turn into a conduction electron) and the catalytic activity of heterogeneous catalysts.[5] Cu-oxides (Cu_2O and CuO) have low bandgap energy, *ca.* 1.3–2.5 eV. They are known for their high catalytic activity,[6] along with their non-toxic nature and affordability, cause these Cu-oxides to be studied intensively.[7] With the developments in colloidal synthesis, the control of size, shape, morphology, and composition of metal oxide nanoparticles is possible. Various symmetrical morphologies, including cubic, octahedral and rhombic dodecahedral Cu_2O and CuO nanocrystals, have been prepared.[5, 8–13] Additionally, structurally more complex versions of these well-defined symmetrical shapes, such as truncated octahedral and truncated cubes, can also be prepared.[14–17] Since it is well known that controlled morphology is key in enhancing the catalytic properties of heterogeneous catalysts,[18] Cu_2O and CuO nanocrystals catalyst with a definite shape and size can be prepared. This control allows for facet and morphologically dependant catalytic studies.

This study wanted to explore the use of Cu-oxide nanocrystals with a definite shape and size for the catalytic reduction of various nitrophenols using $NaBH_4$. Nitrophenols are among others side-products formed during the preparation of pesticides, herbicides and synthetic dyes,[19–21] which are hazardous to living organisms. Hydrogenation of these nitrophenols to aromatic amines turn these environmentally redundant compounds into useful intermediates and precursors for pharmaceuticals, polymers, pigments and agrochemicals.[22–24]

The as-prepared catalyst's morphology and chemical composition/oxidation state on the surface was investigated by SEM, UV-vis, XRD, ATR FTIR and XPS, respectively. The structural and chemical stability/changes of the Cu-oxide nanocrystals upon oxidation, reduction, and catalytic activity were explored.

2. Experimental

2.1. Chemicals

The solid and liquid reagents (from Sigma-Aldrich and Merck) were used without purification. Double-distilled water was used where necessary. XPS data were recorded on a PHI 5000 Versaprobe system with a monochromatic Al Kα X-ray source. The surface morphology and the elementary composition were investigated using a Shimadzu Superscan ZU SXX-550 electron microscope (SEM), coupled with an energy dispersive X-ray spectroscope (EDS). A Bruker Tensor 27 (equipped with a diamond crystal) was used to examine wavenumber positions with ATR-FTIR of the neat crystal. UV-Vis characterisation of the Cu-oxide nanocrystals in suspension was measure on an Olis Clarity CCD UV/Vis Spectroscopic system. This system can measure the UV-Vis of suspended material since it can eliminate the effect of light scatter and thus allows accurate absorbance of turbulent solutions. It has an effective path length of 30 cm; thus, the Beer–Lambert law does not apply. The XRD pattern of the prepared truncated cubic Cu-oxide nanocrystals was recorded on a Bruker D8 Advance diffractometer, using a Cu Kα radiation in the range 25–85°. The UV-Vis spectra of the kinetics were recorded in a Cary 50 Probe UV/Visible spectrophotometer.

2.2. Preparations

2.2.1. Colloidal synthesis of truncated cubic Cu_2O

The truncated cubic Cu_2O was prepared by a modified method based on the method of Z. Zhang et al.[5] $CuCl_2$ (298 mg, 2.2 mmol) was dissolved in 175 ml water. This solution was heated to 55 °C, and 17.5 ml of a 2 M NaOH solution was added dropwise. The solution was allowed to stir for a further 30 min at 55 °C, followed by the dropwise addition of 17.5 ml of 0.6 M ascorbic acid. The solution was allowed to stir for a further 5 h

*To whom correspondence should be addressed
Email: erasmuse@ufs.ac.za

ISSN 1996-840X Online / South African Chemical Institute / http://saci.co.za/journal

https://doi.org/10.17159/0379-4350/2021/v75a12

at 55 °C. The precipitate was filtered and washed with water. After drying in a vacuum oven, the product was obtained in 44% (138.5 mg) yield.

2.3. Reduction of nitrophenols using $NaBH_4$

5 ml Nitrophenols (200 ppm) was added to 70 ml water in a round bottom flask. 5 ml Freshly prepared $NaBH_4$ (0.1 M, 19 mg in 5 ml water) was added to the water mixture. The time was started when 10 mg of the truncated cubic Cu_2O catalyst was added. A UV-Vis spectrum was collected at suitable time intervals.

3. Results and Discussion

The truncated cubic Cu-oxide nanocrystals were prepared by a colloidal synthesis procedure using ascorbic acid to direct structure growth. The hybrid morphological features of these Cu-oxide nanocrystals could be determined from Scanning Electron Microscopy (SEM) images, see Figure 1 (Left). The truncated cubic Cu-oxide is enclosed by six {100} facets on the basal planes of the cube, while twelve {110} facets enclose the edges of the cube and eight {111} facets are located on the corners (see Figure 1 (middle) for a cartoon illustrating this). These Cu-oxide nanocrystals are monodispersed and fairly uniform, with an average edge length of 600 nm (see the Supplementary Information (Fig. 1S) for the histogram and related data).

The crystallinity and phase purity of the truncated cubic Cu-oxide nanocrystals were analysed by X-ray Diffraction (XRD). The XRD pattern of the Cu-oxide nanocrystals is present in Figure 1 (Right). The reflections at 29.1°, 35.9°, 41.8°, 52.0°, 60.9°, 73.1° and 76.9° are attributed to the {110}, {111}, {200}, {211}, {220}, {311} and {222} facets of the truncated cubic Cu-oxide, respectively. The reflections are at slightly lower degrees (*ca.* 0.5°) than that found for cubic Cu_2O,[25] which is attributed to the structure having the truncated system. The presence of the truncated cubic Cu-oxide nanocrystals in the Cu_2O form was confirmed. However, a small amount of Cu^0 was also detected at 34.7°, 41.9°, 52.2° and 73.3° in correlation to published results.[26] The peak relating to the Cu^0 appeared as a small shoulder of the main peak resulting from the Cu_2O form (see insert Figure 1 (Right)). This peak indicates that the truncated cubic Cu-oxide nanocrystals are not exclusively present in the Cu^I state but that some Cu^0 is also present. No CuO (Cu^{II} state) was detected since no peak was detected at *ca.* 32.5°, which is the position where the strong {110} peak appears.[27] X-ray photoelectron spectroscopy (XPS) analysis was conducted on the truncated cubic Cu-oxide nanocrystals sample to confirm this finding further.

XPS was used to determine the atomic composition and oxidation state of the copper and the ratio of the different atomic species present on the surface of the nanocrystals. The wide scan spectra (showing all the elements present) is given in the Supplementary Information (Figure S2 (A)). These photoelectron lines were charge corrected by shifting the spectra so that the lowest binding energy of the simulated adventitious carbon C 1s photoelectron line is set at 284.8 eV. The peak maximum of the Cu 2p envelopes were found at *ca.* 932 and 952 eV for the Cu $2p_{3/2}$ and Cu $2p_{1/2}$ photoelectron lines, with small shake-up features at *ca.* 10-12 eV higher than the main photoelectron lines (Figure S2 (B)). These shake-up features typically correspond to the presence of Cu^{II}, either as CuO or $Cu(OH)_2$. Due to the difficulty distinguishing between metallic Cu, Cu^I (in Cu_2O) and Cu^{II} (in CuO or $Cu(OH)_2$), the curve fitting parameter proposed by Biesinger[28] was employed to identify the species present. The visual representation of the simulated curve-fitting parameters used (relative binding energy, relative ratio of Full Width at Half Maximum and relative atomic %) as per Cu species is presented in Figure 2 (A). Simultaneously, the Table with the numerical data can be found in reference no. 28. The simulated fits imposed on the XPS data of the as-prepared truncated cubic Cu-oxide nanocrystals using the fitting parameters of Biesinger are shown in Figure 2 (B), and the data are summarised in Table 1. This fit confirms the XRD data, where metallic Cu (most probably inside the particle) and Cu_2O (in the Cu^I state) covering the outside of the particle is present. $Cu(OH)_2$ (in the Cu^{II} state) was also observed in the XPS. However, the XRD analysis did not detect the characteristic peaks of $Cu(OH)_2$ (strongest peak presents at *ca.* 31.2°).[29] The relative percentages of the different species present are 52.0% of Cu_2O, 30.9% Cu^0 and 17.1% $Cu(OH)_2$.

In literature, it has been described that Cu_2O (Cu(I)) nanoparticles can be oxidised to CuO (Cu(II)) upon exposure to air.[30] This oxidation is reported to be size-dependent; the smaller the nanoparticles, the more reactive they are for oxidisation in

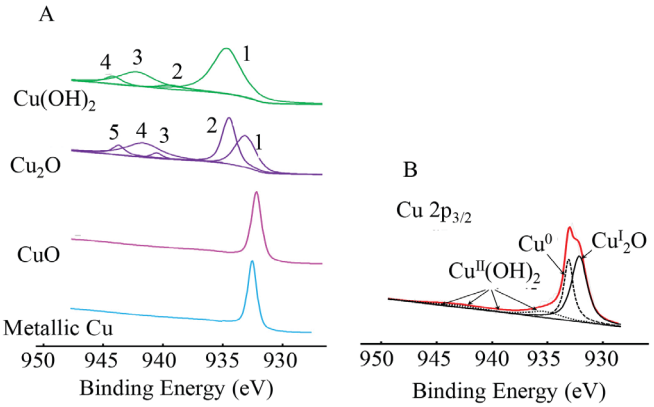

Figure 2 (A) A graphical representation of the simulated fitting parameters suggested by Biesinger,[28] the simulated fitted peaks in the spectra of $Cu(OH)_2$ and CuO shows the numerical labels used to assign the XPS binding energy data presented in Table 1. (B) The detail XPS scan of the Cu $2p_{3/2}$ area of the truncated Cu-oxide nanocrystals, showing the simulated fittings.

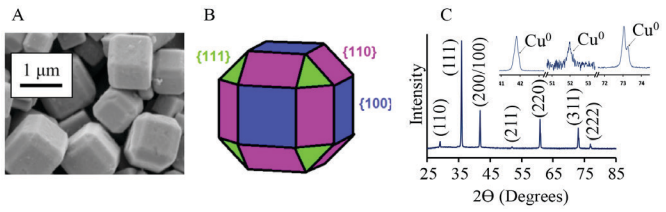

Figure 1 The SEM images (A), a cartoon indicating the facets enclosing the particle (B) and the XRD pattern (C) of the as-prepared truncated cubic Cu-oxide nanocrystals.-

Table 1 Cu $2p_{3/2}$ simulated curve-fitting parameters of the as-prepared truncated cubic Cu-oxide nanocrystals after treatment with $NaBH_4$. The numerical peaks labels correlate with the simulated fitted peaks in Cu(OH)2 and CuO spectra shown in Figure 2.

		As prep	$NaBH_4$
BE Cu_2^IO (eV)		932.1	
% ratio		52.0	
BE Cu(0) (eV)		933.0	932.56
% ratio		30.9	100
BE $Cu^{II}(OH)_2$ (eV)	Peak 1	935.2	
	Peak 2	939.8	
	Peak 3	942.7	
	Peak 4	944.7	
Total % ratio		17.1	

air. It is also mentioned that bulk Cu_2O is not stable in air at room temperature and can easily be oxidised. However, this stability was not observed for the truncated cubic Cu-oxide nanocrystals (average edge length 600 nm) as verified by the absence of Cu(II) in the XPS and XRD. The O 1s oxygen peak of the truncated cubic Cu-oxide nanocrystals was also fitted with the suggested simulation parameters of Biesinger,[28] see Figure S3 in the Supplementary Information. The O 1s photoelectron line of the Cu_2O and $Cu(OH)_2$ was found at 530.4 and 531.8 eV, respectively.

The UV-Visible spectra of the Cu-oxide nanocrystals suspended in water exhibited a broad absorption peak with two local maximum points located at 454 and 472 nm (see Figure 3, A). The latter compares very well with the reported wavelength of maximum absorption of cubic Cu-oxide suspended in ethanol, found at 470 nm.[31]

The classical Tauc equation[32] was employed to determine the apparent bandgap energy, E_g', of the Cu-oxide nanocrystals (the term apparently is used since this is not a thin film but nanocrystals):

$$\alpha E_p = K(E_p - E_g)^{1/2}$$

where α is the absorption coefficient (α = ln(T/d), where T = transmission and d = thickness, average edge length was used in this case), K is a constant, E_p is photon energy ($E_p = hc/\lambda$, h = Planck's constant and c = speed of light), and E_g is the bandgap energy. The extrapolated value (E_p at α = 0) of the straight line to the X-axis of the graph of $(\alpha E_p)^2$ versus E_p represents the apparent bandgap energy, which was found to be $E_g' = 2.07$ eV (see Figure S4 in the Supplementary Information).

Figure 3 (B) shows the ATR FTIR spectrum of truncated cubic Cu-oxide nanocrystals. The transmittance frequency peak at 1105 cm^{-1} is attributed vibrational band of the -O-H group (of $Cu(OH)_2$), in correlation with published results.[33] The presence of this peak further confirms that $Cu(OH)_2$ is present in the sample. The lower frequency peaks at 700 cm^{-1} and 607 cm^{-1} are assigned to the Cu-O stretching frequency in Cu_2O.[34,35]

The nanocrystals were exposed to $NaBH_4$ to investigate the reduction of the Cu^I present in the Cu_2O to metallic Cu^0. Furthermore, since the model catalytic type reactions that will be tested is the reduction of nitrophenols with $NaBH_4$, the influence of the $NaBH_4$ on the Cu-oxide nanocrystals is important. The same experimental conditions as during the catalysis were applied except that the nitrophenols were absent (10 ml of a 6.25 mM $NaBH_4$ solution was added to a 70 ml suspension of the Cu-oxide nanocrystals (10 mg)). The SEM image indicates that individual cubic structures were maintained. However, the well-defined edges had been smoothed (Figure 4 (A)). As for the chemical composition (as measured by XPS, see Figure 4 (B) for the Cu $2p_{3/2}$ area), the Cu^I converted 100% to metallic Cu^0 with the new binding energy at 932.56 eV.

The heterogeneous catalytic activity of the truncated cubic Cu-oxide nanocrystals, with sodium borohydride ($NaBH_4$), was evaluated for the reduction of three different nitrophenols. The nitrophenols under investigation were 2-, 3- and 4-nitrophenol. The time-dependent absorption curves (Figure 5) show a decrease in the absorption at the peak maxima in the visible region. Manipulation of the data resulted in the construction of the absorption vs time (at the wavelength of peak maxima) and $\ln(A/A_0)$ vs time graphs (Figure 5). The later graph exhibited a linear relationship, having a negative slope. The absolute value of the slope is the apparent pseudo-first-order rate constant (see Table 2 for the average of the experiment done in triplicate),[36] which will be used to compare the reduction rates of the different nitrophenols. The order of reactivity from slowest to fastest is:

4-Nitrophenol < 3-Nitrophenol < 2-Nitrophenol

Comparison of the apparent pseudo-first-order rate constant, k', with the Hammett constants (an empirical value relating the reaction rates and equilibrium constants of meta- and para-substituted aromatic compounds)[37] of the different nitrophenol revealed a linear relationship (see Table 2 for the data and Fig. 5S in the Supplementary Information for the graph). This relationship showed that an increase in the Hammett constant is associated with an increase of k'. A higher Hammett constant is associated with a stronger electron-withdrawing effect (implying more electron density on the nitro-group). This

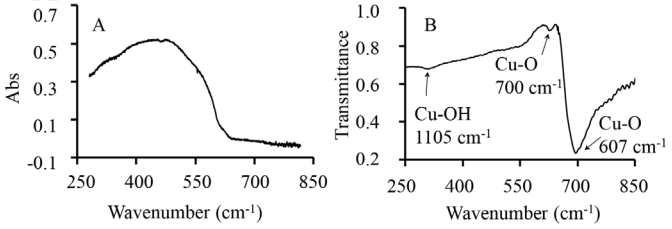

Figure 3 (A) The UV-Visible spectra of the truncated cubic Cu-oxide nanocrystals (1 mg/8 ml water). (B) ATR FTIR spectrum of neat truncated cubic Cu-oxide nanocrystals.

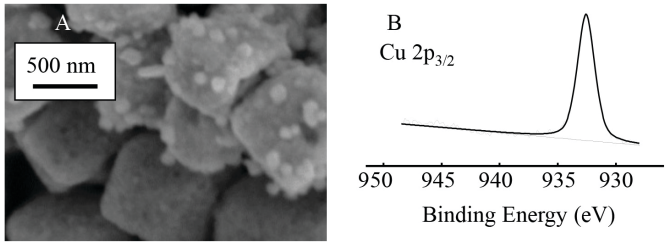

Figure 4 (A) The SEM images of the truncated cubic Cu-oxide nanocrystals after exposure to $NaBH_4$. (B) The detailed XPS of the Cu $2p_{3/2}$ region of the truncated cubic Cu-oxide nanocrystals after exposure to $NaBH_4$.

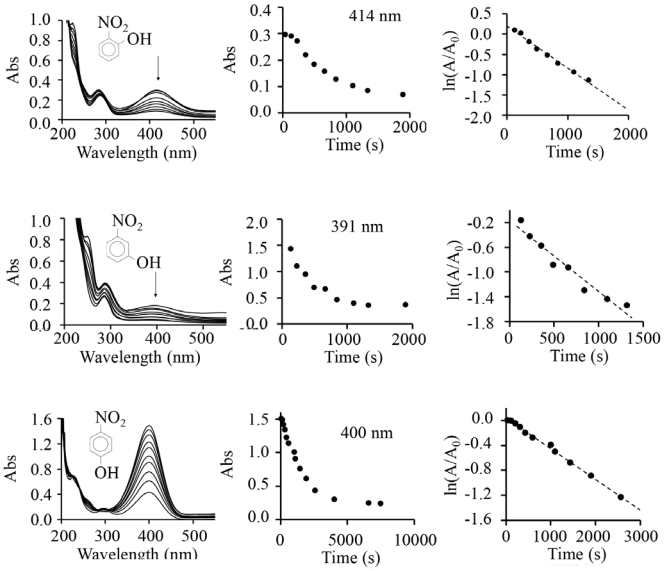

Figure 5 The UV-Vis absorption spectra over time, the graph of absorption vs time at the given wavelength and the graphs of the $\ln(A/A_0)$ vs time (from which the apparent rate constants were calculated for comparison) for the catalytic reduction of 2-, 3- and 4-nitrophenol over the truncated cubic Cu-oxide nanocrystals using $NaBH_4$ as the reducing agent.

Table 2 Kinetic data of the comparative study of the catalytic reduction of 2-, 3- and 4-nitrophenol over the truncated cubic Cu-oxide nanocrystals using $NaBH_4$ as the reducing agent, showing the wavelength at the measured peak maxima (nm) and the apparent pseudo-first-order rate constant, k', (s^{-1}). The Hammett constants of the nitro groups in different positions on the aromatic ring are also tabulated.

Nitrophenols	Wavelength (nm)	Apparent pseudo-first-order rate constant, k', (s^{-1})	Hammett constants[38]
2-Nitrophenol	414	1.16×10^{-3}	1.24
3-Nitrophenol	391	5.72×10^{-4}	0.71
4-Nitrophenol	400	5.11×10^{-4}	0.78

effect suggests that the larger electron density causes faster reduction rates of the nitrophenol (over the truncated cubic Cu-oxide nanocrystals using $NaBH_4$ as the reducing agent). These reduction rates are due to the easier nucleophilic attack of the oxygen (of the nitro group) on the H^+, caused by the increased electron density. This attack trend is similar to what was obtained for the electrochemical reduction of nitrophenol with the nitro groups in different positions.[38]

The apparent pseudo-first-order rate constants halved when the recovered catalyst (truncated cubic Cu-oxide nanocrystals) was used for a second catalytic cycle. After one catalytic cycle, the recovered catalyst's SEM image revealed that the particles retain their global cubic structure, but the planes and edge are no longer smooth (Figure 6, (A)). This reduced smoothness corresponds to the surface degradation of the truncated cubic Cu-oxide nanocrystals exposed to $NaBH_4$ (see Figure 4). This loss in the catalytic activity of the truncated cubic Cu-oxide nanocrystals correlates to the literature[39], where it was reported that cubic Cu-oxide nanocrystals showed a significant loss in catalytic activity (for an oxidative arylation reaction) after the first cycle, from 94% to 47% yield. Li *et al.*[39] also found the degradation of the straight edges attributed to the dissolution and reconstruction of active atoms at corners or edges during catalysis. In analogue to this, it is proposed that during the catalytic reduction of nitrophenol, some of the active Cu-oxide fragments break away from the truncated cubic Cu-oxide nanocrystals. Subsequently, these smaller particles aggregate randomly to the large Cu-oxide particle. The decreased activity of truncated cubic Cu-oxide nanocrystals could be due to the loss of active atoms into the reaction mixture.

After the second catalytic cycle, the SEM image showed that needle-like nanostructures protrude from the surfaces of the rough "cubic" structures (Figure 6 (B)). XPS measurements of the recovered catalysts revealed that only metallic Cu^0 (binding energy Cu $2p_{3/2}$ = 932.56 eV) was present in the recovered catalyst sample. Similar to when the truncated cubic Cu-oxide nanocrystals were treated with $NaBH_4$, and there was no evidence of Cu^I of Cu^{II} species in the materials.

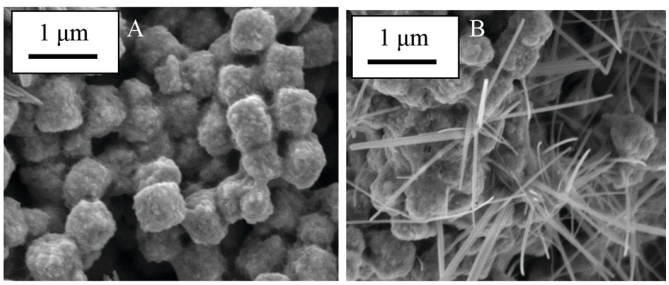

Figure 6 (A) The truncated cubic Cu-oxide's SEM images after one cycle and (B) two cycles of catalytic reduction of 4-nitrophenol using $NaBH_4$.

4. Conclusion

Herewith we have disclosed the successful preparation of truncated cubic Cu-oxide nanocrystals with a *ca.* 600 nm edge length. The detailed morphologies of the polyhedral structures were characterised by XRD and SEM, while the chemical and physical properties were analysed by UV-Vis, ATR FTIR, and XPS.

The XRD pattern indicates that the truncated cubic Cu-oxide nanocrystals are not exclusively present in the Cu^I state but that some Cu^0 is also present. The XPS confirmed this presence, revealing some Cu^{II} present in the $Cu(OH)_2$ form. The structure and chemical composition are unstable towards exposure to the reducing agent $NaBH_4$. Treatment with $NaBH_4$ reduced the Cu^I fully to metallic Cu^0. The sharp and well-defined facets of the truncated cubic structure's edge and corners were lost and became round.

The truncated cubic Cu-oxide nanocrystals can be used as a catalyst for reducing a variety of different nitrophenols. The order of reactivity from slowest to fastest is:

4-Nitrophenol < 3-Nitrophenol < 2-Nitrophenol

A directly proportional relationship was obtained between the pseudo-first-order rate constant, k', and the Hammett constants of the different nitrophenol. This relationship implies that an increase in the electron-withdrawing ability of the nitrophenol (higher Hammett constant) results in a faster reaction (an increase of k').

The recovered catalyst was found to be in the metallic Cu^0 state, which was not as active as the Cu_2O state. The structure deformed from the truncated cube to a "fussy" cubic structure after one cycle. After a second cycle, the SEM revealed that needle-like nanostructures protrude from the surfaces of rough "cubic" structures.

Acknowledgements

The author would like to acknowledge generous financial support from Sasol and the UFS during this study. Dr Shaun Cronjé from the Physics Department at the UFS is acknowledged for the XRD measurements.

Supplementary Material

Supplementary information for this article is provided in the online supplement.

ORCID iD

Elizabeth Erasmus: https://orcid.org/0000-0003-0546-697X

References

1 M. Kazes, D. Y. Lewis, and U. Banin, Method for preparation of semiconductor quantum-rod lasers in a cylindrical microcavity, *Adv. Funct. Mater.*, 2004, **14**(10), 957–962. DOI: 10.1002/adfm.200400018.

2 J. Choi, Y. Jun, S.-I. Yeon, H. C. Kim, J.-S. Shin, and J. Cheon, Biocompatible heterostructured nanoparticles for multimodal biological detection, *J. Am. Chem. Soc.*, 2006, **128**(50) 15982–15983. DOI: 10.1021/ja066547g.

3 C. Xu *et al.*, Au–Fe_3O_4 dumbbell nanoparticles as dual-functional probes, *Angew. Chemie Int. Ed.*, 2008, **47**(1), 173–176. DOI: 10.1002/anie.200704392.

4 J. C. Vedrine, *Metal Oxides in Heterogeneous Catalysis*, 1st edn, Elsevier, Amsterdam, 2018.

5 A. Bean Getsoian, Z. Zhai, and A. T. Bell, Band-gap energy as a descriptor of catalytic activity for propene oxidation over mixed metal oxide catalysts, *J. Am. Chem. Soc.*, 2014, **136**(39), 13684–13697. DOI: 10.1021/ja5051555.

6 Y. Wang *et al.*, Electronic structures of Cu_2O, Cu_4O_3, and CuO: A joint experimental and theoretical study, *Phys. Rev. B*, 2016, **94**(24), p. 245418. DOI: 10.1103/PhysRevB.94.245418.

7 L. Yu, X. Y. Yu, and X. W. D. Lou, The design and synthesis of hollow micro-/nanostructures: present and future trends, *Adv. Mater.*, 2018,

30(38), 1800939. DOI: 10.1002/adma.201800939.

8 T. Aditya, J. Jana, N. K. Singh, A. Pal, and T. Pal, Remarkable facet selective reduction of 4-nitrophenol by morphologically tailored (111) faceted Cu_2O nanocatalyst, *ACS Omega*, 2017, **2**(5), 1968–1984. DOI: 10.1021/acsomega.6b00447.

9 W. Huang, Oxide nanocrystal model catalysts, *Acc. Chem. Res.*, 2016, **49**(3), 520–527. DOI: 10.1021/acs.accounts.5b00537.

10 Y.-H. Won and L. A. Stanciu, Cu_2O and Au/Cu_2O particles: surface properties and applications in glucose sensing, *Sensors*, 2012, **12**(10), 13019–13033. DOI: 10.3390/s121013019.

11 Y. Zhang, B. Deng, T. Zhang, D. Gao, and A.-W. Xu, Shape effects of Cu_2O polyhedral microcrystals on photocatalytic activity, *J. Phys. Chem. C*, 2010, **114**(11), 5073–5079. DOI: 10.1021/jp9110037.

12 X. Liang, L. Gao, S. Yang, and J. Sun, Facile synthesis and shape evolution of single-crystal cuprous oxide, *Adv. Mater.*, 2009, **21**(20), 2068–2071. DOI: 10.1002/adma.200802783.

13 Y. Sui *et al.*, Low temperature synthesis of Cu_2O crystals: Shape evolution and growth mechanism, *Cryst. Growth Des.*, 2010, **10**(1), 99–108. DOI: 10.1021/cg900437x.

14 Z. Yang, S. Sun, C. Kong, X. Song, and B. Ding, Designated-tailoring on {100} facets of Cu_2O nanostructures: From pctahedral to its different truncated forms," *J. Nanomater.*, 2010, **2010**, 1–11, DOI: 10.1155/2010/710584.

15 E. Erasmus, Morphology-dependent Ullmann C-O arylation using Cu_2O nanocrystals, *J. Nanomater.*, 2020, **2020**, 1–7. DOI: 10.1155/2020/6726170.

16 J. Zeng *et al.*, Facile synthesis of cubic cuprous oxide for electrochemical reduction of carbon dioxide, *J. Mater. Sci.*, 2021, **56**(2), 1255–1271. DOI: 10.1007/s10853-020-05278-y.

17 A. Aljaafari, N. Parveen, F. Ahmad, M. W. Alam, and S. A. Ansari, "Self-assembled Cube-like Copper Oxide Derived from a Metal-Organic Framework as a High-Performance Electrochemical Supercapacitive Electrode Material," *Sci. Rep.*, vol. 9, no. 1, p. 9140, Dec. 2019, DOI: 10.1038/s41598-019-45557-6.

18 D. Astruc, "Introduction: Nanoparticles in catalysis," *Chem. Rev.*, 2020, **120**(2), 461–463. DOI: 10.1021/acs.chemrev.8b00696.

19 S. Panigrahi *et al.*, Synthesis and size-selective catalysis by supported gold nanoparticles: Study on heterogeneous and homogeneous catalytic process, *J. Phys. Chem. C*, 2007, **111**(12), 4596–4605. DOI: 10.1021/jp067554u.

20 C. V. Rode, M. J. Vaidya, and R. V. Chaudhari, Synthesis of p -aminophenol by catalytic hydrogenation of nitrobenzene, *Org. Process Res. Dev.*, vol. 3, no. 6, pp. 465–470, Nov. 1999, DOI: 10.1021/op990040r.

21 N. Comisso *et al.*, Electrodeposition of Cu–Rh alloys and their use as cathodes for nitrate reduction, *Electrochem. Commun.*, 2012, **25,** 91–93. DOI: 10.1016/j.elecom.2012.09.026.

22 K. B. Narayanan and N. Sakthivel, Synthesis and characterisation of nano-gold composite using *Cylindrocladium floridanum* and its heterogeneous catalysis in the degradation of 4-nitrophenol, *J. Hazard. Mater.*, 2011, **189**(1–2), 519–525. DOI: 10.1016/j.jhazmat.2011.02.069.

23 T.-L. Lai, K.-F. Yong, J.-W. Yu, J.-H. Chen, Y.-Y. Shu, and C.-B. Wang, High efficiency degradation of 4-nitrophenol by microwave-enhanced catalytic method, *J. Hazard. Mater.*, 2011, **185**(1), 366–372.x DOI: 10.1016/j.jhazmat.2010.09.044.

24 D. Makovec, M. Sajko, A. Selišnik, and M. Drofenik, Magnetically recoverable photocatalytic nanocomposite particles for water treatment, *Mater. Chem. Phys.*, 2011, **129**(1–2), 83–89. DOI: 10.1016/j.matchemphys.2011.03.059.

25 S. Kumar *et al.*, Facile synthesis of hierarchical Cu2O nanocubes as visible light photocatalysts, *Appl. Catal. B Environ.*, 2016, **189**, 226–232. DOI: 10.1016/j.apcatb.2016.02.038.

26 N. A. Dhas, C. P. Raj, and A. Gedanken, Synthesis, Characterisation, and Properties of Metallic Copper Nanoparticles, *Chem. Mater.*, 1998, 10(5), 1446–1452. DOI: 10.1021/cm9708269.

27 M. Černík and V. V. Thekkae Padil, Green synthesis of copper oxide nanoparticles using gum karaya as a biotemplate and their antibacterial application, *Int. J. Nanomedicine*, 2013, **8**, 889–898. , DOI: 10.2147/IJN.S40599.

28 M. C. Biesinger, Advanced analysis of copper X-ray photoelectron spectra, *Surf. Interface Anal.*, 2017, **49**(13), 1325–1334. DOI: 10.1002/sia.6239.

29 H. K. A. J. V. K. M. H. Sabzevar, Facile synthesis of copper oxide nanoparticles using copper hydroxide by mechanochemical process, *J. Ultrafine Grained Nanostructured Mater.*, vol. 48, pp. 37–44, 2015, DOI: 10.7508/jufgnsm.2015.01.006.

30 G. Cheng and A. R. H. Walker, Transmission electron microscopy characterisation of colloidal copper nanoparticles and their chemical reactivity, *Anal. Bioanal. Chem.*, 2009, **396**(3), 1057–1069. DOI: 10.1007/s00216-009-3203-0.

31 L. Chen *et al.*, Copper salts mediated morphological transformation of Cu_2O from cubes to hierarchical flower-like or microspheres and their supercapacitors performances, *Sci. Rep.*, 2015, **5**(1), 9672. DOI: 10.1038/srep09672.

32 J. Tauc, *Amorphous and Liquid Semiconductors*. Springer, Boston, MA US, 1974.

33 D. P. Dubal, G. S. Gund, C. D. Lokhande, and R. Holze, CuO cauliflowers for supercapacitor application: Novel potentiodynamic deposition, *Mater. Res. Bull.*, 2013, **48**(2), 923–928. DOI: 10.1016/j.materresbull.2012.11.081.

34 K. Borgohain, J. B. Singh, M. V. Rama Rao, T. Shripathi, and S. Mahamuni, Quantum size effects in CuO nanoparticles, *Phys. Rev. B*, 2000, **61**(16), 11093–11096. DOI: 10.1103/PhysRevB.61.11093.

35 E. C. Heltemes, Far-infrared properties of cuprous oxide, *Phys. Rev.*, 1966, **141**(2), 803–805. DOI: 10.1103/PhysRev.141.803.

36 N. Sreeju., A. Rufus, and D. Philip, Microwave-assisted rapid synthesis of copper nanoparticles with exceptional stability and their multifaceted applications, *J. Mol. Liq.*, 2016, **221**, 1008–1021. DOI: 10.1016/j.molliq.2016.06.080.

37 S. L. Keenan, K. P. Peterson, K. Peterson, and K. Jacobson, Determination of Hammett equation rho constant for the Hydrolysis of p-nitrophenyl benzoate esters," *J. Chem. Educ.*, 2008, **85**(4), 558. DOI: 10.1021/ed085p558.

38 Y. Jiang, X. Zhu, H. Li, and J. Ni, Effect of nitro substituent on electrochemical oxidation of phenols at boron-doped diamond anodes, *Chemosphere*, 2010, **78**(9), 1093–1099. DOI: 10.1016/j.chemosphere.2009.12.036.

39 L. Li, C. Nan, Q. Peng, and Y. Li, Selective synthesis of Cu_2O nanocrystals as shape-dependent catalysts for oxidative arylation of phenylacetylene," *Chem. - A Eur. J.*, 2012, **18**(34), 10491–10496. DOI: 10.1002/chem.201200567.

Supplementary material to:

E. Erasmus

Truncated edge cuprous oxide cube architecture for reduction of nitrophenols

S. Afr. J. Chem., 2021, **75**, 106–110

Truncated edge cuprous oxide cube architecture for reduction of nitrophenols

Elizabeth Erasmus

SUPPLEMENTARY INFORMATION

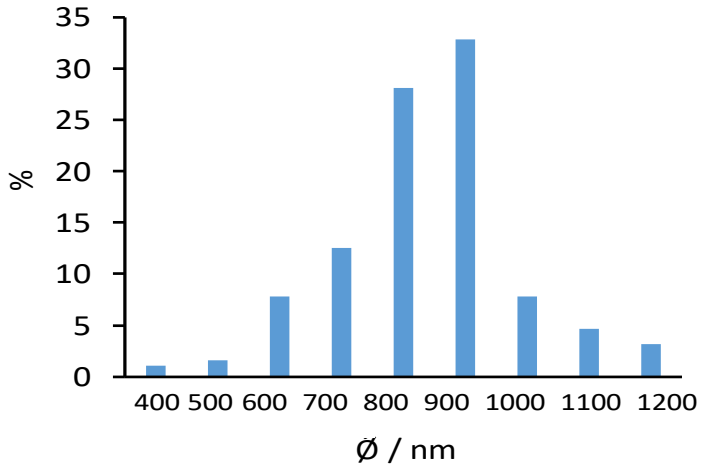

Mean (nm)	600
Minimum (nm)	340
Maximum (nm)	1173
Standard deviation (nm)	217

Figure S1. Left: The histogram showing the distribution of the measured particle sizes. Right: The table showing the mean, minimum and maximum diameter (in nm) as well as the standard deviation of the particles as measured from the TEM images of the Cu-oxide nanocrystals.

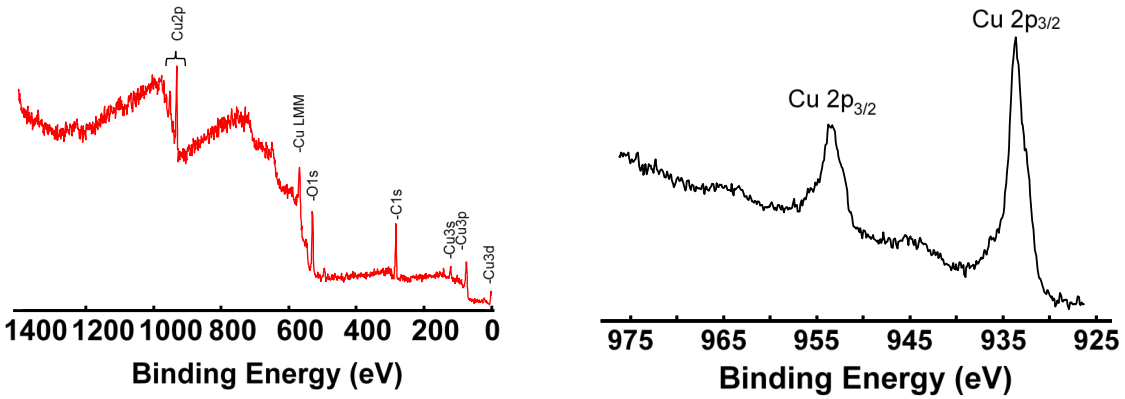

Figure S2. XPS Wide scan of the Cu-oxide (Left) and XPS detail scan of the Cu 2p area of the truncated Cu-oxide nanocrystal (Right).

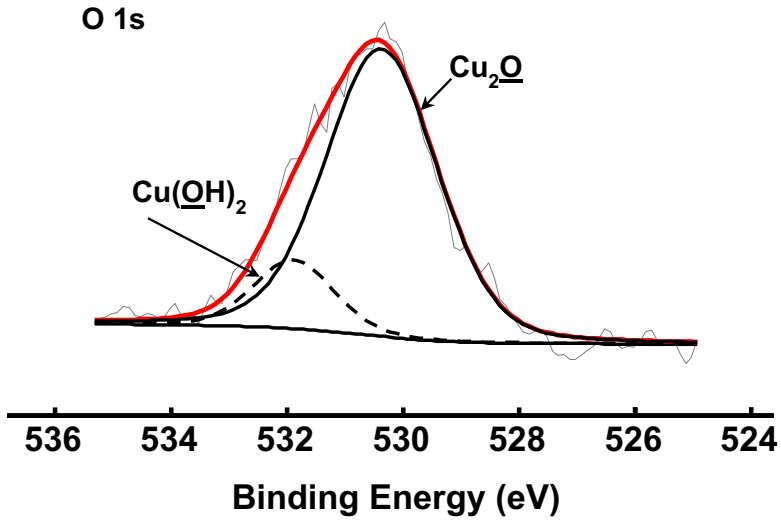

Figure S3. XPS detail scan of the O 1s area of the truncated Cu-oxide nanocrystals, showing the simulated fits.

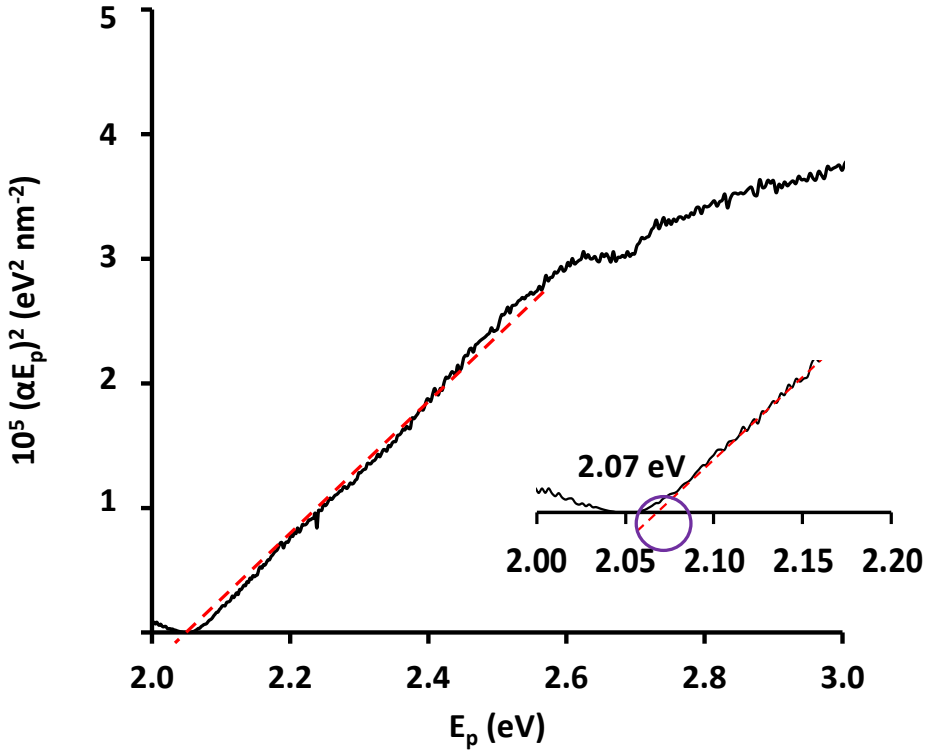

Figure S4. The Tauc plot of $(\alpha E_p)^2$ vs E_p, corresponding to the UV-Vis spectrum in Figure 3.

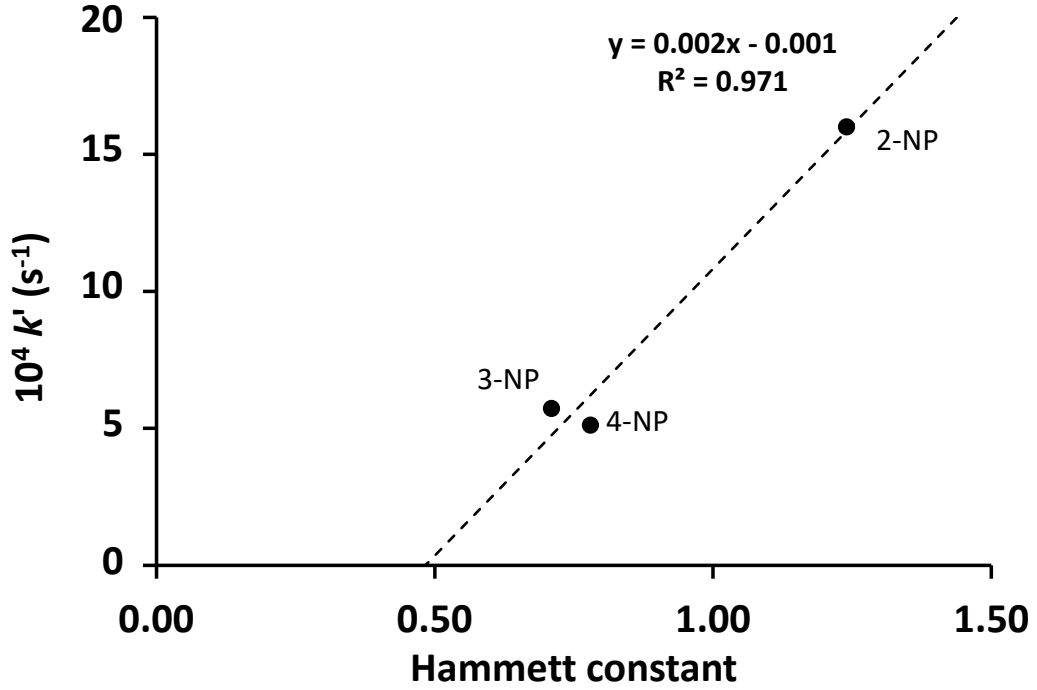

Figure S5. The relationship between the Hammett constants and the apparent pseudo-first-order rate constant, *k*', of the catalytic reduction of 2-, 3- and 4-nitrophenol over the truncated cubic Cu-oxide nanocrystals using $NaBH_4$ as the reducing agent.